

# Technology Development towards WFIRST-AFTA Coronagraph

Ilya Poberezhskiy<sup>a\*</sup>, Feng Zhao<sup>a</sup>, Xin An<sup>a</sup>, Kunjithapatham Balasubramanian<sup>a</sup>, Ruslan Belikov<sup>b</sup>, Eric Cady<sup>a</sup>, Richard Demers<sup>a</sup>, Rosemary Diaz<sup>a</sup>, Qian Gong<sup>c</sup>, Brian Gordon<sup>a</sup>, Renaud Goullioud<sup>a</sup>, Frank Greer<sup>a</sup>, Olivier Guyon<sup>c</sup>, Michael Hoenk<sup>a</sup>, N. Jeremy Kasdin<sup>d</sup>, Brian Kern<sup>a</sup>, John Krist<sup>a</sup>, Andreas Kuhnert<sup>a</sup>, Michael McElwain<sup>c</sup>, Bertrand Mennesson<sup>a</sup>, Dwight Moody<sup>a</sup>, Richard Muller<sup>a</sup>, Bijan Nemati<sup>a</sup>, Keith Patterson<sup>a</sup>, A.J. Riggs<sup>d</sup>, Daniel Ryan<sup>a</sup>, Byoung-Joon Seo<sup>a</sup>, Stuart Shaklan<sup>a</sup>, Erkin Sidick<sup>a</sup>, Fang Shi<sup>a</sup>, Nicholas Siegler<sup>a</sup>, Remi Soummer<sup>f</sup>, Hong Tang<sup>a</sup>, John Trauger<sup>a</sup>, J. Kent Wallace<sup>a</sup>, Xu Wang<sup>a</sup>, Victor White<sup>a</sup>, Daniel Wilson<sup>a</sup>, Karl Yee<sup>a</sup>, Hanying Zhou<sup>a</sup>, Neil Zimmerman<sup>d</sup>

<sup>a</sup>Jet Propulsion Laboratory, Caltech, 4800 Oak Grove Dr., Pasadena, CA 91109

<sup>b</sup>NASA Ames Research Center, Space Science and Astrobiology, Moffett Field, CA 94035

<sup>c</sup>University of Arizona, Steward Obs., 933 North Cherry Ave, Tucson, AZ 85721

<sup>d</sup>Princeton University, MAE, D207 Engineering Quad, Princeton, NJ 08544

<sup>e</sup>NASA Goddard Space Flight Center, Code 667, Greenbelt, MD 20771

<sup>f</sup>Space Telescope Science Institute, 3700 San Martin Drive, Baltimore, MD 21218

## ABSTRACT

NASA's WFIRST-AFTA mission concept includes the first high-contrast stellar coronagraph in space. This coronagraph will be capable of directly imaging and spectrally characterizing giant exoplanets similar to Neptune and Jupiter, and possibly even super-Earths, around nearby stars. In this paper we present the plan for maturing coronagraph technology to TRL5 in 2014-2016, and the results achieved in the first 6 months of the technology development work. The specific areas that are discussed include coronagraph testbed demonstrations in static and simulated dynamic environment, design and fabrication of occulting masks and apodizers used for starlight suppression, low-order wavefront sensing and control subsystem, deformable mirrors, ultra-low-noise spectrograph detector, and data post-processing.

**Keywords:** WFIRST-AFTA, stellar coronagraph, exoplanet direct imaging, exoplanet spectral characterization, shaped pupil coronagraph, hybrid lyot coronagraph, low order wavefront sensor, deformable mirror, integral field spectrograph

## 1. INTRODUCTION

### 1.1 WFIRST-AFTA Coronagraph Overview

A Wide Field Infrared Space Telescope (WFIRST) was the top-ranked priority for a large space mission in the New Worlds/New Horizons (NWNH) report of the 2010 National Academy of Sciences Decadal Survey for Astronomy. After a 2.4 meter optical telescope assembly (OTA) was made available to NASA, it became the basis for the WFIRST mission study. The new concept, termed WFIRST-AFTA (Astrophysics Focused Telescope Assets) also added a coronagraph instrument to the baseline mission configuration. This coronagraph will be capable of directly imaging companions to the nearby bright stars down to contrast ratios of  $10^{-9}$  and angular separations between  $\sim 0.1$  and 2 arcseconds, depending on the wavelength. The integral field spectrograph will acquire spectra of these companions with resolution of  $R \sim 70$  over the wavelength range of 600-980 nm. Equipped with such an instrument, WFIRST-AFTA will be able to characterize a number of known Radial Velocity (RV) planets, discover several new Jupiter and Neptune-type exoplanets, and also detect and characterize debris disks in systems containing a few times the solar system's level of zodiacal dust. In addition to producing valuable science output, the WFIRST-AFTA coronagraph will be flown as a technology demonstration to advance exoplanet direct imaging and characterization technologies as a step towards a future New Worlds telescope that will discover and analyze nearby Earth-like exoplanets.

More information about the WFIRST-AFTA coronagraph instrument is available in the proceedings of this conference, including the general instrument overview [1], description of the current flight design concept [2], and the most recent science output estimates [3]. The scope of this paper is to describe our plan for maturing the technologies necessary to make flight implementation of the coronagraph a reality within the timeline envisioned by NASA, and our current status in each of the relevant technology areas.

The AFTA Coronagraph Working Group (ACWG), with representatives from the Exoplanet Program Office (ExEPO), WFIRST Study Office (WSO) and Science Definition Team (SDT) worked between June and December of 2013 to comprehensively assess several candidate coronagraph architectures. During this activity, the coronagraphs were evaluated according to their expected performance and science return [4], technology maturity and likelihood of meeting the key program gates on schedule, and the ability to fit and perform within the spacecraft and telescope constraints.

Based on the information from the ACWG and a report from the independent Technology Advisory Committee (TAC), the NASA Science Mission Directorate (SMD) selected the Occulting Mask Coronagraph (OMC) – a combination of a Hybrid Lyot Coronagraph (HLC) and a Shaped Pupil Coronagraph (SPC) in a single instrument – as the baseline for WFIRST-AFTA, with the Phase-Induced Amplitude Apodization Complex Mask Coronagraph (PIAA-CMC) as the backup technology. The OMC design fits into the specified volume/mass/power envelope and has a relatively small increase in complexity compared to either the SPC and HLC instrument configurations alone. Its advantages include risk mitigation during the technology development phase and in-flight, due to the trade-off between greater robustness to pointing jitter provided by SPC and greater exoplanet science return promised by HLC.

The WFIRST Coronagraph Science Definition Team (SDT) is presently working on finalizing the initial version of coronagraph Level 1 requirements, expected to be released later in the summer of 2014. Key preliminary coronagraph parameters are listed in Table I.

Table I. WFIRST-AFTA Coronagraph Key Parameters (Preliminary)

<b>Parameter</b>	<b>Target Value</b>	<b>Comments</b>
Imaging Bandpass	430 – 1000 nm	Measured sequentially in five ~10% bands (TBR)
Inner Working Angle	110 – 250 mas	~3λ/D, driven by science and limited by coronagraph capability and/or pointing jitter
Outer Working Angle	0.9 – 2 arcsec	Limited by 48x48 DM
Detection Limit	Planet Contrast ≤ 10 <sup>-9</sup> (after post-processing)	Cold Jupiters and Neptunes, not exo-Earths. Deeper contrast looks unlikely due to pupil shape and stability requirements
Spectral Resolution	~70	With IFS, R~70 across 600–980 nm (TBR)
IFS Spatial Sampling	17 mas	3 samples per diffraction limit at λ~600nm

## 1.2 Description of Key Coronagraph Technologies

The coronagraph instrument conceptual block diagram is shown in Fig. 1. It shows light from the Optical Telescope Assembly (OTA) first delivered to the coronagraph instrument's Tertiary Module (TM), which includes a Fast Steering Mirror (FSM) that corrects pointing jitter and drift using feedback from the Low Order Wavefront Sensor (LOWFS). The light is then sent to two 48x48 actuator Deformable Mirrors (DMs), which perform active wavefront control to compensate for phase and amplitude imperfections in the optical train and, particularly in the HLC case, mitigate the impact of the telescope pupil obscurations. DM actuators are controlled by a high-order electric field estimation and correction algorithm which typically runs prior to the observation to maximize starlight suppression. The heart of the coronagraph is the starlight suppression system specific to each coronagraph architecture, which not only prevents the starlight from reaching the imaging sensor and spectrograph, but also sends the bulk of the rejected starlight to the LOWFS subsystem where it is used to extract the pointing error and wavefront drift information. A flip mirror can send the planet light and residual starlight to either the imaging channel for planet detection and high order wavefront control or to the Integral Field Spectrograph (IFS) for planet characterization.

We are focusing our attention in 2014-2016 on maturing the technologies marked with a star:

1. Starlight suppression components, such as SPC apodizer and HLC occulting mask
2. Coronagraph system demonstration
3. Deformable mirrors
4. IFS Focal Plane Array (FPA)
5. Low order wavefront sensing and control
6. Data post-processing

The objectives to the coronagraph team set by WSO and NASA HQ management are to advance novel coronagraph technologies and retire key engineering risks by September 30, 2016, bringing the coronagraph to NASA Technology Readiness Level (TRL) 5. In the following sections we describe our plan for meeting these objectives and the progress achieved in the first 6 months since the architecture downselect.

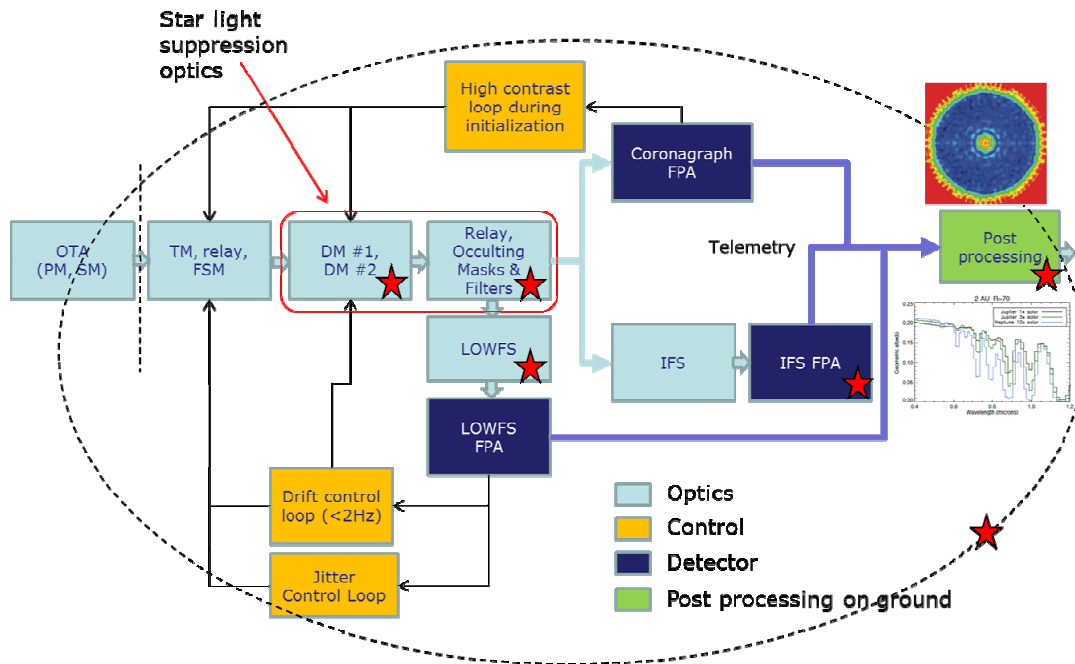


Fig. 1. Block diagram of the coronagraph system showing the key optical components, detectors and control loops. Stars indicate technology areas whose maturation is prioritized for the WFIRST-AFTA coronagraph.

## 2. STARLIGHT SUPPRESSION TESTBED DEMONSTRATIONS AND COMPONENTS

### 2.1 Sequence of Coronagraph Testbed Demonstrations

Demonstrations of WFIRST-AFTA coronagraph technologies will be started on the “static” testbeds, which refers to the fact that no intentional wavefront disturbances are introduced before the coronagraph. The block diagram of such a testbed is shown in Fig. 2(a). During the static test phase, we validate the novel designs, fabrication approaches, and workmanship of the key starlight suppression components (masks and apodizers), deformable mirror performance, as well as high-order wavefront estimation and control algorithms that are necessary to meet the coronagraph contrast vs. working angle requirements.

In the beginning, the coronagraph components are designed for a central wavelength of 550 nm, with the intent of later demonstrating coronagraph performance at the other relevant wavelengths. The experimental demonstrations initially employ monochromatic or narrowband light, followed by broadband (at least 10%) demonstrations that use a super-continuum laser source. During the static phase in 2014 through early 2015, the Shaped Pupil Coronagraph, Hybrid Lyot Coronagraph, and PIAA-CMC have separate experimental setups on optical tables inside vacuum tanks. Resource allocation is prioritized for the two primary OMC technologies.

During the second “dynamic” phase of the experimental demonstrations, an OTA simulator is added to the system to introduce realistic jitter and low-order wavefront drift expected on the WFIRST-AFTA observatory. A LOWFS/C subsystem is integrated with the coronagraph to sense and correct these wavefront disturbances, with the experimental block diagram shown in Fig 2(b). At this stage, the previously separate HLC and SPC setups will be combined into one OMC dynamic coronagraph testbed that is convertible between HLC and SPC modes of operation. This validation of coronagraph performance – contrast and throughput vs. working angle – that meets instrument science requirements, in

broadband light, with realistic input wavefront disturbances will be the lynchpin of TRL5 demonstration by September 2016. Our recent progress for each of the coronagraph technologies is described in sections 2.2-2.4.

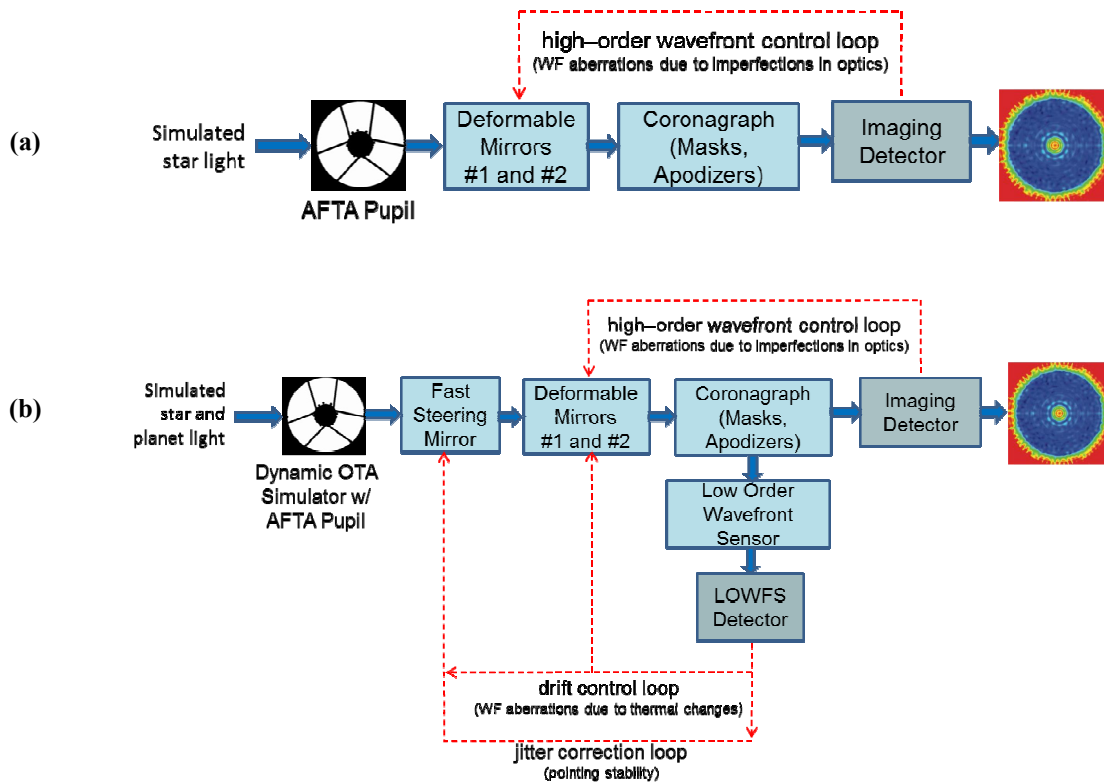


Fig. 2. Block diagram of the coronagraph testbed demonstration setups in (a) static and (b) dynamic environments.

In the 4<sup>th</sup> quarter of 2015, NASA Goddard Space Flight Center is scheduled to deliver a prototype IFS to JPL, where it will be integrated with the coronagraph, initially on a static testbed and subsequently on the dynamic OMC testbed [5]. The IFS utilizes a lenslet array followed by a pinhole array mask to achieve high intrascene contrast. Its preliminary design is shown in Fig. 3 and the requirements are listed in Table II. We will validate IFS performance with the coronagraph and provide the experimentally obtained datacubes to the data post-processing team.

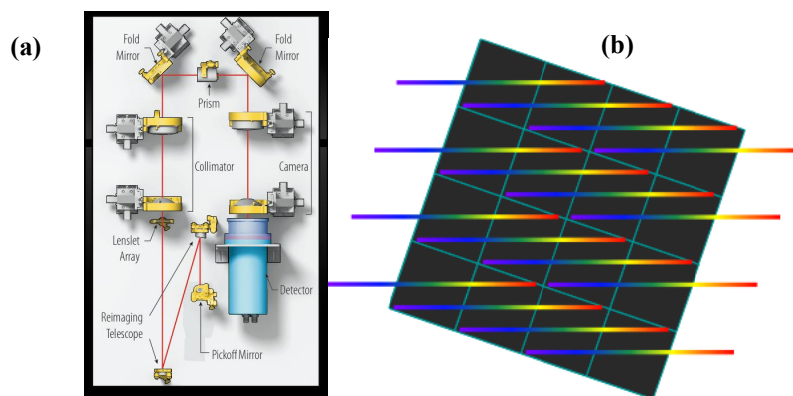


Fig. 3. (a) Preliminary conceptual design of the testbed IFS, and (b) illustration of the concept used for separating the spectra of different spatial elements on the IFS detector.

Table II. Testbed Integral Field Spectrograph Specifications.

Description	Units	Required Value	Comment
Spatial (lenslet) sampling	lenslets per lambda/D @ 600nm	3 to 5	Must Nyquist sample at all wavelengths
Instrument spectral bandpass	nm	600 to 1000	
Instantaneous spectral bandpass ( $\Delta\lambda_{bandwidth}/\lambda$ )	%	20	
Number of bands		3	650, 800, 950 nm centers
Spectral resolution ( $\lambda/\delta\lambda_{res}$ )		70	
Outer working angle	arcsec	950nm: 1.6 600nm: 1.0	Driven by radial location of spectroscopy targets
Utilized detector area	pixels	1024×1024	
Detector pixel pitch	μm	13	

## 2.2 Shaped Pupil Coronagraph

The shaped pupil coronagraph is one of the two technologies comprising the OMC instrument. It was pioneered by the High Contrast Imaging Laboratory at Princeton University [6-9]. Shaped pupil has a relatively simple architecture and uses an optimized binary pupil mask to diffract on-axis starlight in a way that creates a dark hole in the PSF. A field stop in the image plane blocks the bulk of the starlight outside the dark hole, while the slightly off-axis planet light is passed through the field stop and then reimaged onto a detector. Thus, the starlight suppression is largely achieved by the pupil mask, with DM wavefront control further improving the coronagraph performance, and the field stop reducing the signal dynamic range on the detector.

Previously, shaped pupil coronagraphs have demonstrated high contrast performance in a testbed:  $\sim 2 \times 10^{-9}$  in 10% broadband light at  $\sim 4\lambda/D$  working angle [10]. They have also demonstrated 2-DM operation [7]. Shaped pupil can accommodate various telescope pupil shapes [6,8,9] and is relatively insensitive to observatory jitter. The pupil mask itself is achromatic.

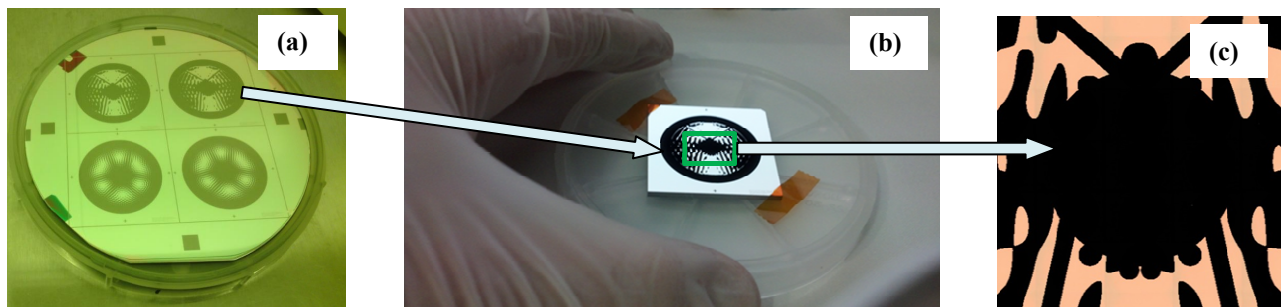


Fig. 4. Reflective shaped pupil: (a) a processed wafer with 2 discovery and 2 characterization masks, (b) a fabricated characterization mask, (c) design details showing absorbing black silicon and highly reflective aluminum. Colored tints on (a) and (c) are caused by microscope illumination.

The shaped pupil masks designed for the WFIRST-AFTA telescope pupil have small “island” features and are not suitable for the traditionally used transmissive mask fabrication approach [11]. A new reflective mask approach was developed and validated at JPL, with high reflectivity aluminum regions and absorbing black silicon regions (Fig. 4),

produced on a silicon wafer. Several iterations of masks using this approach have been fabricated at JPL and Caltech, with significant quality improvements along the way. A characterization mask, designed to produce two 60° dark holes was delivered to the SPC static testbed in April of 2014. This mask underwent extensive stand-alone characterization for a variety of imperfections and analysis/modeling of their expected impact on coronagraph contrast, with encouraging results that are summarized in Table III.

Table III. Reflective Shaped Pupil Mask Characterization Results.

Mask Imperfection Type	Measured Level	Predicted Change in Contrast after WFC (modeling/analysis)	Comments
Black Si reflectivity, specular	$<7 \times 10^{-8}$	$<2.1 \times 10^{-10}$	Upper bound; limited by measurement setup
Black Si reflectivity, diffuse	$<0.6\%$	$<10^{-11}$	
Mask wavefront error	$\sim 0.036\lambda$ rms (above focus)	$7 \times 10^{-11}$	- Post WF control - Better wafers received
Isolated defects	Small pinholes and 2 scratches	$8 \times 10^{-12}$	Post WF control
Al reflectivity variations	$\sim 0.5\%$	Correctable with $<1\%$ of DM stroke	- Post WF control, - Variations on SP similar to other coron. Optics
<b>Total</b>		$<3 \times 10^{-10}$	<b>Upper bound</b>

Good preliminary results have been obtained in the static shaped pupil testbed, initially using monochromatic light at 516 nm, as shown in Fig. 5. These results are expected to show further improvement in the future. Since two deformable mirrors were not available in the spring of 2014, we started experimental work with 1 DM, producing a one-sided dark hole as a result. A conversion to a 2-DM configuration is planned for late summer of 2014, with transition to broadband experiments planned in 2014 as well.

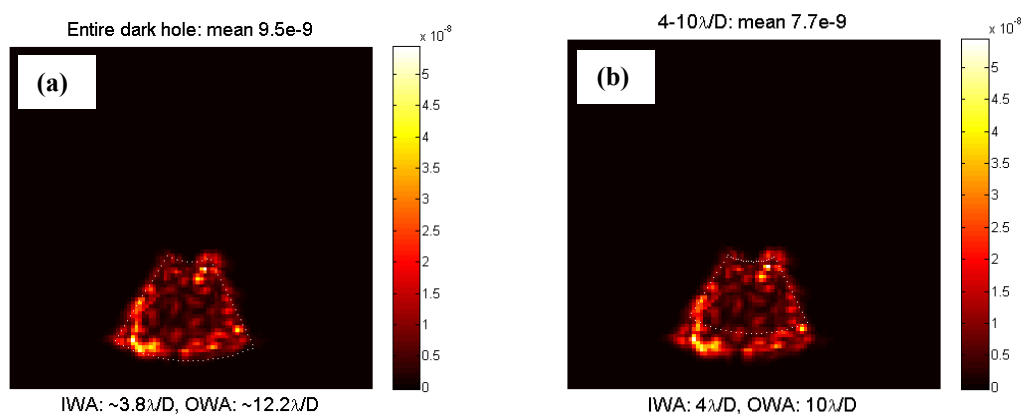


Fig. 5. Preliminary shaped pupil results obtained using a characterization mask in May 2014 with a monochromatic source. The light outside the dark hole is blocked by a field stop. A single-sided dark hole is created since only 1 DM was available to start the test. (a) Contrast averaged in the entire transmitted field and (b) contrast excluding area outside 10  $\lambda/D$  working angle where there are no known WFIRST-C targets.

The biggest challenge for the shaped pupil has been achieving aggressive IWA (which is a key to reaching the maximum number of RV exoplanet targets), higher contrast, and higher throughput. While the fabrication and testbed

characterization results described above have been obtained with the shaped pupil designs generated in the fall of 2013, a design improvement effort at Princeton has been making significant progress. New SPC modifications have been proposed with a greater contrast and more aggressive inner working angle that will result in improved science performance, while continuing to rely on the recently proven fabrication techniques. These newer SPC designs will be later validated on the SPC testbed.

### 2.3 Hybrid Lyot Coronagraph

The main starlight suppression component in a Hybrid Lyot Coronagraph is a focal plane occulting mask with optimized layers of metal and dielectric [10, 12-14]. The metal in the mask reflects the majority of the incoming on-axis starlight, and diffracts the transmitted starlight so that it is blocked by the Lyot stop in a downstream pupil plane, while the slightly off-axis planet light is transmitted to the imaging detector or the integral field spectrograph.

Hybrid Lyot coronagraph and its bandlimited predecessor have previously demonstrated the highest reported laboratory contrast results [10, 12], exceeding  $10^{-9}$  in a 10% band at  $\sim 3\lambda/D$  working angle. Coronagraph designs used in these past demonstrations were optimized for an unobscured telescope pupil and used linear occulting masks to create a one-dimensional (and one-sided due to the use of 1 DM) dark hole. Thus the main challenges in the transition from the older coronagraphs to the WFIRST-AFTA HLC have been two-fold: (1) to create a design that achieves high broadband contrast with the obscured pupil of the AFTA 2.4 meter telescope and in presence of realistic observatory jitter and (2) fabricate for the first time a circular occulting mask. Substantial progress on both fronts has been achieved.

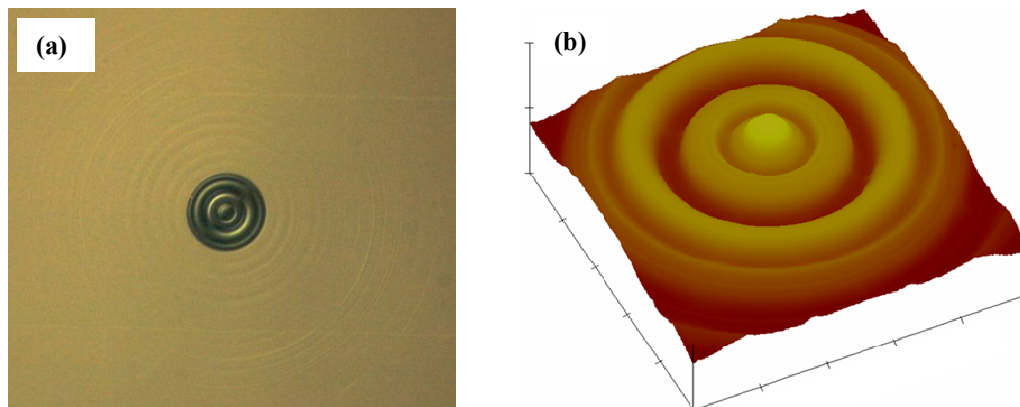


Fig. 6. A prototype of the HLC circular occulting mask imaged with (a) differential interference contrast microscope, (b) atomic force microscope image of the central portion only.

The initial HLC design started during the ACWG downselect process in 2013, and since then design revisions, consisting of optimizing both the occulting mask profile and deformable mirror settings, resulted in significant improvements in the following areas:

1. Predicted contrast performance at small inner working angles in realistic observatory jitter environment has been greatly enhanced, with the corresponding improvement of the exoplanet science output.
2. The profiles of metal and dielectric layers have been simplified to make their fabrication less challenging for the existing fabrication approaches.
3. Compatibility with LOWFS mask: A preliminary study was conducted indicating that the Hybrid Lyot mask can be combined with a Zernike wavefront sensor phase mask, retaining high performance on the part of both the coronagraph and the wavefront sensor. Further HLC mask optimization with the LOWFS mask “built-in” will be performed in the future.
4. DM stroke minimization: Fixed actuator patterns on the 2 DMs are critical to the way Hybrid Lyot coronagraph deals with the telescope pupil obscurations from the secondary mirror and supporting spiders. However, large

static DM stroke has negative consequences, for example reducing the effective throughput of the coronagraph. The rms DM stroke has been reduced in recent HLC design iterations.

Significant progress has also been achieved in the fabrication of HLC occulting masks. In Fig. 6, a circular HLC mask prototype made at JPL is shown. HLC testbed and mask will be ready to begin static testing in August 2014, utilizing from the start two 48x48 DMs that are baselined for the flight instrument.

## 2.4 Backup PIAA-CMC Coronagraph Technology

The backup PIAA-CMC technology is based on the PIAA concept of apodizing the telescope pupil using reflections from two carefully shaped aspheric mirrors [15]. A variation of PIAA called PIAA-CMC was proposed for the WFIRST-AFTA coronagraph with easier-to-make aspheric mirrors and a phase mask with a number of concentric rings in the focal plane [16]. The PIAA-CMC concept promised the greatest science return during the downselect, but had less technical heritage and was somewhat more complex than the two primary approaches. Since the downselect, PIAA-CMC phase mask fabrication capabilities and limitations have been investigated, and an updated PIAA-CMC instrument design will be delivered and evaluated in July of 2014.

## 2.5 Low Order Wavefront Sensing and Control

To achieve the required coronagraph performance in a realistic space environment, a Low Order Wavefront Sensing and Control (LOWFS/C) subsystem is necessary. This subsystem provides sensing and suppression of (a) spacecraft pointing drift and jitter and (b) low order wavefront errors driven by changes in thermal loading of the telescope and the rest of the observatory.

LOWFS/C performance will be initially validated in a dedicated LOWFS/C testbed, before its components are integrated into the dynamic OMC testbed. The validated system will include an OTA simulator that injects realistic pointing jitter and low-order wavefront error drift in the optical path, as well as LOWFS/C which provides sensing and closed-loop suppression of these wavefront disturbances to levels that enable the coronagraph to meet its science requirements. Sensing information can also be used for PSF subtraction and data editing. Closed loop control will be used to suppress i) pointing jitter using a Fast Steering Mirror (FSM) with ~50 Hz control bandwidth and ii) several low-order wavefront error terms using a DM or actuated powered optics.

The coronagraph team began by defining several needs and wants for the LOWFS system, such as:

1. LOWFS will use the starlight rejected by the coronagraph.
2. LOWFS will use a common light pick-off point for both OMC technologies – a focal plane with HLC occulters and SPC field stops.
  - a. If possible, LOWFS masks will be combined with the coronagraph masks to minimize non-common path errors.
3. LOWFS will use a single, high frame rate, low noise camera to sense tip/tilt and low order wavefront error
4. LOWFS will rely on mature, space qualified components, such as camera and fast steering mirror for tip/tilt correction. While this is not a must for the testbed, it is desirable for flight traceability.

To develop LOWFS requirements, the impact of thermal changes during realistic observing scenarios on low order wavefront error and ultimately the coronagraph contrast was modeled. Then two sensing concepts were compared in-depth: Zernike wavefront sensor [17] and masked-PSF wavefront sensor [18]. The following parameters were used to conduct this trade:

1. Noise equivalent angle vs. stellar magnitude
2. Noise equivalent low-order (Z4-Z11) wavefront error vs. stellar magnitude
3. Wavefront error capture range
4. Sensing linearity
5. LOWFS mask optimal design parameters and manufacturing tolerances
6. Feasibility of combining LOWFS mask with HLC and SPC focal plane masks

Target star magnitudes ranging from 0 to 8 were considered, with the understanding that fainter stars will require longer integration times to achieve the required sensing accuracy. Both sensor concepts delivered excellent performance. The Zernike wavefront sensor (Fig. 7) was ultimately selected primarily because it can be combined with (profiled on top of) both HLC and SPC masks. Design work for the testbed LOWFS system and the OTA simulator is currently under way. They will be validated in early 2015 in a stand-alone LOWFS/C setup and then incorporated into the dynamic OMC testbed.

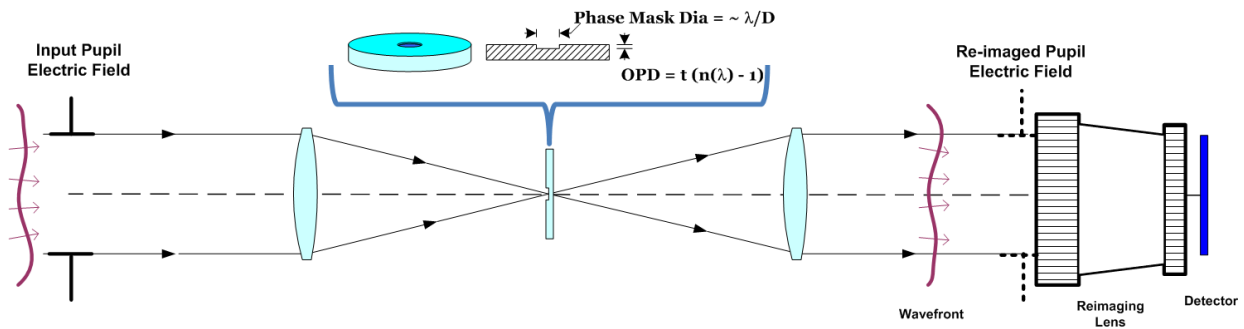


Fig. 7. Conceptual diagram of the selected Zernike wavefront sensor. The phase mask will be used in reflection and combined with OMC focal plane masks.

### 3. COMPONENT MATURATION

#### 3.1 Deformable Mirror

WFIRST-AFTA coronagraph instrument has baselined the monolithic PMN (Lead Magnesium Niobate) Deformable Mirror (DM) technology developed by AOA Xinetics (AOX) [19]. JPL has a long history of working with Xinetics to develop large format, small actuator pitch PMN DMs for high contrast imaging [20]. Such mirrors were used in the highest contrast testbed demonstrations of all Lyot-type coronagraphs: HLC, SPC, PIAA, and Vector Vortex [10]. Two 48x48, monolithic PMN DMs were manufactured by Xinetics for the first time and delivered to JPL in 2009 (Fig. 8a) with the following specifications:

Table IV. AFTA-C Baseline Deformable Mirror Specifications.

Parameter	Specifications	Notes
Array size	48 x 48	
Actuator spacing	1 mm	
Stroke range	0.5um	
Actuator capacitance	50nF	Nominal
Drive voltage range	0 – 100V	Typical bias voltage 30V to 50V
Facesheet material	Fused Silica	
Coating	Bare Aluminum	
Unpowered surface figure	10nm rms	
Influence function at nearest neighbor	10%	
Hysteresis	<1%	Hysteresis of PMN actuator developed for this product is temperature sensitive; listed specifications is for room temperature operation
Number of bad actuators in circle of 48 actuator diameter	0	
Electrical connection interface	Custom 48x50 pin-grid array	Integrated at JPL

One of these two DMs successfully passed a random vibration test with an overall level of 10.8 g rms in 2012. This test level was based on a survey of random vibration proto-flight test levels for 10 relevant JPL missions. Both DMs are being integrated and tested in HCIT. A new DM currently on order from AOX will be subjected to further environmental testing in 2014 in an effort to advance this DM technology to TRL6.

In parallel, a new generation DM driver for HCIT has been designed and fabricated to move from multiplexed to non-multiplexed drivers (Fig. 8b). This change is aimed at alleviating the problem of stroke drift experienced by actuators with lower parallel resistance during multiplexing. A flight version of non-multiplexed driver is under development.

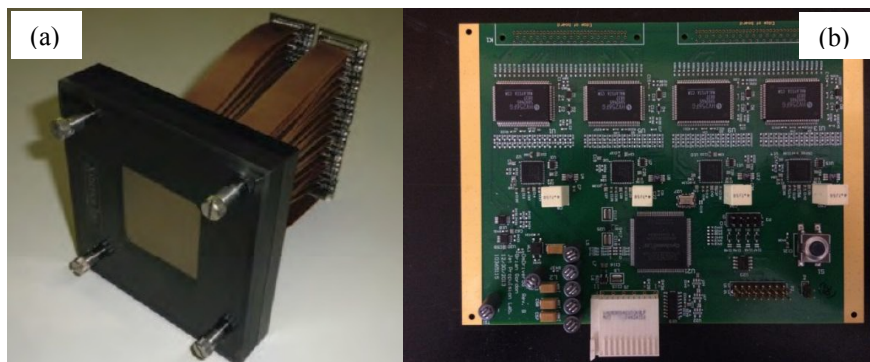


Figure 8: (a) 48x48 PMN deformable mirror with 24 flex ribbon and connectors, (b) new generation 128 channel, non-multiplexed, DM driver board.

### 3.2 Integral Field Spectrograph Detector

Detector specifications for the integral field spectrograph were derived from the following requirements and goals:

1. scientific goal of detecting and characterizing at least six planets in each of three spectral bands (600, 800, and 900nm),
2. mission constraints limiting total spectral observation time to ~100 days (TBR),
3. detector format and size derived from the IFS design, and
4. technology maturity: capability of attaining TRL 6 within two years.

Three candidate detector technologies were identified, which are, in order of descending technology readiness level: scientific CCDs, Electron-Multiplying (EM) CCDs, and scientific CMOS (complimentary metal oxide semiconductor) detectors. In order to derive detector specifications an instrument model was developed to predict the estimated time required to detect and characterize planets in all three spectral bands [21]. The modeling showed that the CCD201 EMCCD from e2v (Fig. 9) outperforms the other candidate detectors and thus it was selected as the baseline for the WFIRST-AFTA coronagraph. A list of preliminary detector specifications – based closely on the CCD201 published specifications – is shown in Table 5. The e2v CCD201 is a standard product with both astronomical and other scientific applications, and can be operated in three different modes, two of which use a high-gain output register to achieve sub-electron effective read noise, which is essential for attaining the science goal of six detected planets. In the third operating mode, the CCD201 can be operated as a standard scientific CCD using a built-in output register.

The current mission baseline plan calls for the CCD201 to be operated as an EMCCD in analog gain mode, however, as a risk mitigation measure, the designed coronagraph camera electronics will be able to read the CCD201 in the standard CCD mode. Operation in this mode is equivalent to flight-proven CCD readout architecture that is used in cameras that successfully operate on HST WFC3, Kepler, and Gaia. In addition, a minor customization of the standard version of the CCD201 is being considered for the WFIRST coronagraph: a version with deep depleted silicon that significantly boosts the quantum efficiency in 900-1000 nm spectral range. Since the flight Gaia red photometry CCDs were fabricated with deep depleted silicon, this is a low risk customization. The WFIRST-AFTA coronagraph project has begun a two-year task for technology maturation and demonstration of CCD201 detectors and camera electronics in the relevant environment.

Table V. AFTA-C IFS Detector Specifications

Requirement	Value	Units	Comments
Read Noise	0.2	e/pix/fr	Effective read noise, incl. EM gain
Dark Current	$5 \times 10^{-4}$	e/pix/sec	Effective dark current, incl. ENF
Clocking-Induced Charge (CIC) Noise	$10^{-3}$	e/pix/frame	Effective CIC, incl. ENF
Area	1000 x 1000	pixels	Minimum Area
QE at (600, 800, 900) nm	(50, 50, 25)	%	Minimum QE

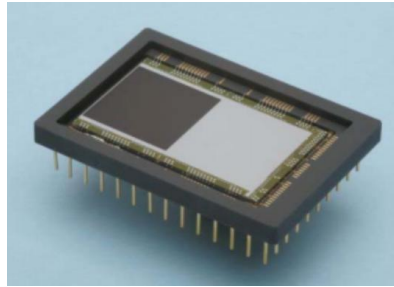


Figure 9. CCD201 detector from e2v.

## 4. ALGORITHM MATURATION

### 4.1 Integrated Modeling of Observing Scenario

Some of the most challenging aspects of coronagraph operation must be studied through an integrated model that takes into account the interplay of observing conditions, the expected changes in thermal and structural loads, and the resulting optical effects. Two of the most pressing aspects are the acquisition of the dark hole and the stability of the speckles once an observation begins.

Coronagraph integrated modeling team is planning on getting a first look at these questions in 2014, by initially defining a representative ('strawman') observing scenario and producing a series of simulated images from the detectors under these conditions. In the initial phase, the scenario will be simple, assuming thermal load changes only affect the telescope and structure, but not the coronagraph assembly. The simulated images will be in two groups: the first will represent the dark hole acquisition, and the second will be a series of images spanning a full integration, with no planet but with starlight speckles. Detector noise will be included in these images. Signal-to-noise of the images will be estimated and compared with basic expectations. In subsequent iterations, integration times will be modified to ensure adequate SNR achieved in each step, and excessive times will be adjusted down. Eventually, the optimal observing sequence simulated data will be evaluated to see if any modifications to the overall observing plan are needed. In addition, the post-processing team will receive simulated data to solve for the speckle structure with noise present.

### 4.2 Data Post-Processing

In order to reach the goal of imaging and spectrally characterizing  $10^{-9}$  contrast exoplanets, WFIRST-AFTA coronagraph is counting on approximately ten-fold contrast improvement from on-ground data post-processing (PP), namely PSF subtraction techniques. While current PP techniques have already achieved contrast improvements of 10x or higher over raw contrast levels of  $10^{-5}$  to  $10^{-3}$  on both ground based and HST coronagraphic data [22-24], their performance has not yet been demonstrated – or studied in sufficient detail – at the much fainter raw contrast levels of WFIRST-AFTA coronagraph. In this context, we have initiated a dedicated PP algorithm development effort with the following main objectives:

- Deliver validated data PP algorithms that demonstrate a contrast enhancement of 10 or higher for both imaging and IFS coronagraphic data. These algorithms will be validated against relevant data sets coming from end-to-end optical simulations and laboratory coronagraphic data obtained from WFIRST coronagraph testbeds.

- In the particular case of the IFS, develop and apply optimum techniques to extract spectral datacubes from IFS raw images. These will incorporate lessons learned from ground-based IFS instruments such as Palomar 1640 [25] and the Gemini Planet Imager [26].
- Help inform and optimize the overall design and observing strategy of the AFTA coronagraph. In particular define the type of speckles diversity and ancillary data to be used for optimum contrast performance.

## 5. CONCLUSION

In the 6 months following NASA's coronagraph technology downselect announcement, WFIRST-AFTA coronagraph team has drafted and begun executing a plan to mature coronagraph technology to TRL5 by September of 2016. Significant progress has been achieved during the first half of 2014. For one primary coronagraph mode, the shaped pupil, a reflective mask with WFIRST-AFTA design has been fabricated, extensively characterized, and validated in a coronagraph testbed with monochromatic light, already producing average contrast exceeding  $10^{-8}$ . We will soon begin validation experiments in broadband light, add a second DM for a 2-sided dark hole, and later will explore more advanced shaped pupil designs that promise to significantly increase the coronagraph science output.

The other primary coronagraph mode, Hybrid Lyot, has improved its design to greatly increase the predicted science output in presence of realistic WFIRST observatory jitter, with deeper contrast at small inner working angles as well as reduced DM stroke resulting in increased throughput. The new design has also reduced mask fabrication complexity; and we have produced, for the first time, circular HLC mask prototypes. The Hybrid Lyot Coronagraph is on track to start testbed demonstration in August of 2014.

The Zernike wavefront sensor was selected for the LOWFS subsystem after an extensive trade study that showed that this concept provides excellent sensing of pointing drift and jitter, as well as low order wavefront drift. Critically, the Zernike mask can be combined with focal plane OMC masks by being fabricated on top of both HLC occulter and SPC field stops. This is important for minimizing non-common path errors between LOWFS and the coronagraph. The LOWFS will use a mature, low-noise, high data rate camera and a flight qualified fast steering mirror.

Key components for the flight instrument have been baselined: a high-heritage deformable mirror with 48x48 PMN-based actuators made by AOX, and an EMCCD detector from e2v for the IFS. The DM is slated to complete its environmental test program in 2014, while the detector will be involved in a program of performance and environmental testing and maturation, which includes the development of flight-traceable read-out focal plane electronics. Finally the integrated modeling and data post-processing efforts are under way, and a prototype integral field spectrograph will be delivered to the coronagraph testbed in late 2015.

## 6. ACKNOWLEDGMENT

This work carried out at the Jet Propulsion Laboratory, California Institute of Technology, was performed under a contract with the National Aeronautics and Space Administration.

## REFERENCES

- [1] Zhao, F., "Overview of WFIRST-AFTA coronagraph instrument," Proc. SPIE, 9143-21, this conference, (2014).
- [2] Goullioud, R., Zhao, F., Tang, H., Rud, M., "The WFIRST-AFTA coronagraph design update," Proc. SPIE, 9143-25, this conference, (2014).
- [3] Traub, W.A., Macintosh, B.A., Kasdin, J.N., Krist, J., Mennesson, B., Savransky, D., Shao, M., Serabyn, E. and Trauger, J. T., "Science yield estimation for AFTA coronagraphs," Proc. SPIE, 9143-20, this conference, (2014).
- [4] Krist, J., "End-to-end numerical modeling of AFTA coronagraphs," Proc. SPIE, 9143-28, this conference, (2014).
- [5] McElwain, M.W., Perrin, M.D., Gong, Q., Wilkins, A.N., Stapelfeldt, K.R., Woodgate, B.E., Brandt, T.D., Heap, S.R., Hilton, G.M., Kruk, J.W., Moody, D., Trauger, J., "PISCES: An integral field spectrograph to advance high contrast imaging technologies," Proc. of SPIE, Vol. 8864, 88641O (2013).
- [6] Carlotti, A., Vanderbei, R., Kasdin, N.J., "Optimal pupil apodizations of arbitrary apertures for high-contrast imaging," Optics Express, Vol. 19, No. 27 / 26796 (2011).

- [7] Riggs, A.J., Groff, T.D., Carlotti, A., Kasdin, N.J., Cady, E.J., Kern, B.D., Kuhnert, A., "Demonstration of symmetric dark holes using two deformable mirrors at the high-contrast imaging testbed," Proc. of SPIE, Vol. 8864, 88640T (2013).
- [8] Carlotti, A., Kasdin, N.J., Vanderbei, R., "Shaped pupil coronagraphy with WFIRST-AFTA," Proc. of SPIE, Vol. 8864, 886410-3 (2013).
- [9] Riggs, A.J.E., Zimmerman, N., Carlotti, A., Kasdin, N.J., Vanderbei, R., "Shaped pupil design for future space telescopes," Proc. SPIE, 9143-69, this conference, (2014).
- [10] Lawson, P. R., Belikov, R., Cash, W., Clampin, M., T. Glassman, T., Guyon, O, Kasdin, N. J., Kern, B. D., Lyon, R., Mawet, D., Moody, D., Samuele, R., Serabyn, E., Sirbu, D., and Trauger, J., "Survey of experimental results in high-contrast imaging for future exoplanet missions," Proc. SPIE, Vol. 8864, 88641F (2013).
- [11] Balasubramanian, K.; Wilson, D.; White, V.; Muller, R., Dickie, M., Yee, K.; Ruiz, R; Shaklan, S.; Cady, E.; Kern, B.; Belikov, R, Guyon, O., Kasdin, N.J., "High contrast internal and external coronagraph masks produced by various techniques," Proc. SPIE 8864, 88641R (2013).
- [12] Trauger, J.T., Moody, D., Gordon, B., Krist, J., Mawet, D., "Complex apodization Lyot coronagraphy for the direct imaging of exoplanet systems: design, fabrication, and laboratory demonstration," Proc. of SPIE, Vol. 8442, 84424Q-1 (2012).
- [13] Trauger, J.T., Moody, D.C., Gordon, B., "Complex apodized Lyot coronagraph for exoplanet imaging with partially obscured telescope apertures," Proc. SPIE, Vol. 8864, 886412-1 (2013).
- [14] Trauger, J.T., Moody, D.C., Gordon, B., "The hybrid Lyot coronagraph for exoplanet imaging and spectroscopy with the WFIRST/AFTA and probe-class space missions," Proc. SPIE, 9143-26, this conference, (2014).
- [15] Guyon, O., Pluzhnik, E.A., Galicher, R., Martinache, F., Ridgway, S.T., and Woodruff, R.A., "Exoplanet Imaging with a Phase-induced Amplitude Apodization Coronagraph. I. Principle," ApJ, Vol. 622, 744 (2005).
- [16] Guyon, O., Belikov, R., Kern, B., Krist, J., Newman, K.E., "PIAA coronagraphy for centrally obscured apertures," Proc. SPIE, 9143-27, this conference, (2014).
- [17] Wallace, J. K., Shanti Rao, S., Jensen-Clem, R. M., Serabyn, G., "Phase-Shifting Zernike Interferometer Wavefront Sensor," Proc. SPIE, Vol. 8126, 81260F (2011).
- [18] Guyon, O., Matsuo, T., and Angel, R., "Coronagraphic low-order wave front sensor: principle and application to a phase-induced amplitude coronagraph," Astrophysical Journal, 693:75–84 (2009).
- [19] Wirth, A., Cavaco, J., Bruno, T., Ezzo, K., "Deformable Mirror Technologies at AOA Xinetics," Proc. of SPIE, Vol. 8780, 87800M (2013).
- [20] Trauger, J., Moody, D., Gordon, B., Gursel, Y., Ealey, M., and Bagwell, R., "Performance of a precision high-density deformable mirror for extremely high contrast imaging astronomy from space," Proc. of SPIE Vol. 4854 (2003).
- [21] Nemati, B., "Detector development for the WFIRST-AFTA coronagraph integral field spectrograph," Proc. SPIE, 9143-23, this conference, (2014).
- [22] Soummer, R. Perrin M.D., Pueyo L., Choquet E., Chen C., Golimowski D.A., Hagan J.B., Mittal, T., Moerchen, M., N'Diaye, M., Rajan, A., Wolff, S., Debes, J., Hines, D. C., and Schneider, G., "Five Debris Disks Newly Revealed in Scattered Light from the Hubble Space Telescope NICMOS Archive," ApJ, 786, 23 (2014).
- [23] Soummer, Pueyo, L., Larkin, J., "Detection and Characterization of Exoplanets and Disks Using Projections on Karhunen-Loève Eigenimages," ApJ, 755, 28 (2012).
- [24] Soummer, R., Hagan, J.B., Pueyo, L., Thormann, A., Rajan, A., Marois, C., "Orbital Motion of HR 8799 b, c, d Using Hubble Space Telescope Data from 1998: Constraints on Inclination, Eccentricity, and Stability," ApJ, 741, 55 (2011).
- [25] Pueyo, L., Crepp, J.R., Vasisht, G., Brenner, D., Oppenheimer, B.R., Zimmerman, N., Hinkley, S., Parry, I., Beichman, C., Hillenbrand, L., Roberts L.C., Dekany, R., Shao, M., Burruss, R., Bouchez, A., Roberts, J., and Soummer, R., "Application of a Damped Locally Optimized Combination of Images Method to the Spectral Characterization of Faint Companions Using an Integral Field Spectrograph," ApJS, 199, 6 (2012).
- [26] Macintosh, B. et al., "The Gemini Planet Imager: First Light," MNRAS, arXiv 1404-2845 (2014).